International Journal of Fluid Mechanics Research, Vol. 32, No. 5, 2005

Natural Convection Flow in a Rotating Fluid Over a Vertical Plate Embedded in a Thermally Stratified High-Porosity Medium[†]

A. J. Chamkha
Manufacturing Engineering Department
The Public Authority for Applied Education and Training
PO Box 42325, Shuweikh, 70654, Kuwait

H. S. Takhar
Engineering Department, Manchester Metropolitan University
Oxford Rd., Manchester, M1 5GD, UK

G. Nath
Department of Mathematics, Indian Institute of Science
Bangalore-560012, India

An analysis has been carried out to study the natural convection flow in a rotating fluid over a vertical plate embedded in a thermally stratified high-porosity medium. The nonlinear coupled parabolic partial differential equations have been solved numerically by using an implicit finite-difference scheme. The flow and temperature fields are strongly influenced by the thermal stratification, porosity, inertia, Rossby number, and Prandtl number, whereas they are weakly dependent on the permeability parameter.

* * *

Nomenclature

a	gradient of the ambient temperature, $\mathrm{K/m}$;
C	dimensionless inertia parameter;
C^*	dimensional inertia parameter, $1/\mathrm{m}$;
C_{fx}	local skin-friction coefficient along the x direction;
C_{fy}	local skin-friction coefficient along the y direction;
g	gravitational acceleration, $\mathrm{m/s^2}$;
Gr_L	Grashof number;
K	dimensionless permeability of the porous medium;
K^*	dimensionless permeability parameter, m^2;

[†] Received 08.08.2005.

ISSN 1064-2277

L characteristic length, m;
Nu local Nusselt number;
$\overline{\mathrm{Nu}}$ average Nusselt number;
Pr Prandtl number;
Ro dimensionless rotation parameter (modified Rossby number);
S dimensionless thermal stratification parameter;
T temperature, K;
T_0 ambient temperature at $x = 0$, K;
T_∞ ambient temperature, K;
T_w wall temperature, K;
u, v, w velocity components along x, y, and z directions, respectively, $\mathrm{m/s}$;
U, V, W dimensionless velocity components along x, y, and z directions, respectively.

Greek Symbols

α_e effective thermal diffusivity of the medium, $\mathrm{m^2/s}$;
β volumetric coefficient of thermal expansion, $1/\mathrm{K}$;
ϵ dimensionless porosity of the medium;
θ dimensionless temperature;
μ dynamic viscosity of the fluid, $\mathrm{kg/(m \cdot s)}$;
ν kinematic viscosity of the fluid, $\mathrm{m^2/s}$;
ρ fluid density, $\mathrm{kg/m^3}$;
Ω angular velocity of the fluid, $1/\mathrm{s}$.

Introduction

Natural convection flow over a vertical surface embedded in porous media is encountered in many engineering problems, such as in the design of pebble-bed nuclear reactors, catalytic reactors and compact heat exchangers, geothermal energy conversion, use of fibrous materials in the thermal insulation of buildings, heat transfer from storage of agricultural products that generate heat as a result of metabolism, petroleum reservoirs, storage of nuclear wastes, etc. Comprehensive reviews of papers on this topic have been presented by Cheng [1, 2], Catton [3], Pop et al. [4], Nield and Bejan [5], Vafai [6], Pop and Ingham [7], and Ingham and Pop [8]. Tien and Vafai [9] have discussed the importance of non-Darcy effects, such as the inertia and boundary effects. Chen et al. [10] have investigated the non-Darcy effects on the natural convection boundary layer flow on an isothermal vertical flat plate placed in a high-porosity medium. Certain porous materials, such as form metals and fibrous media, have a high porosity ($0.9 \geq \epsilon \geq 0.95$). Thermal stratification occurs in cooling ponds, lakes, solar ponds, and in the atmosphere. If the vertical surface is a part of an enclosure, then the ambient temperature of the fluid will be stratified. For stable thermal stratification, the temperature in the ambient fluid increases with height. Singh and Tiwari [11] have studied the non-Darcy natural convection boundary layer flow over a vertical isothermal surface embedded in a thermally stratified fluid-saturated porous medium. The above problem for a highly porous medium was investigated by Chen and Lin [12]. Their analysis was extended by Chamkha [13] to include the effect of a magnetic field. Minto et al. [14] studied the natural convection flow driven by an exothermic reaction over a vertical surface in a porous medium. Jung et al. [15] considered the non-Darcy free convection from a non-isothermal vertical surface in a thermally stratified porous medium. Rees and Pop [16] examined the effect of variable permeability on the natural convection

flow on a vertical plate in a porous medium. Takhar et al. [17] investigated the natural convection flow on a vertical cylinder embedded in a thermally stratified high-porosity medium.

The aim of this analysis is to consider the natural convection flow of a rotating fluid over a heated vertical plate embedded in a high-porosity medium. The non-Darcy effect,s which include the inertia, boundary, and convective effects, are included in the analysis. The nonlinear coupled parabolic partial differential equations governing the flow and heat transfer under boundary layer approximations have been solved numerically using an implicit finite-difference scheme [18]. The results have been compared to those of Chen and Lin [12]. The present results will be useful in the design of catalystic and compact heat exchanges.

1. Analysis

We consider a Cartesian coordinate system (x, y, z) rotating uniformly with the fluid. The heated vertical plate is embedded in a highly porous medium and aligned along the x direction in the xy plane. The fluid away from the plate is rotating with a constant angular velocity Ω about the

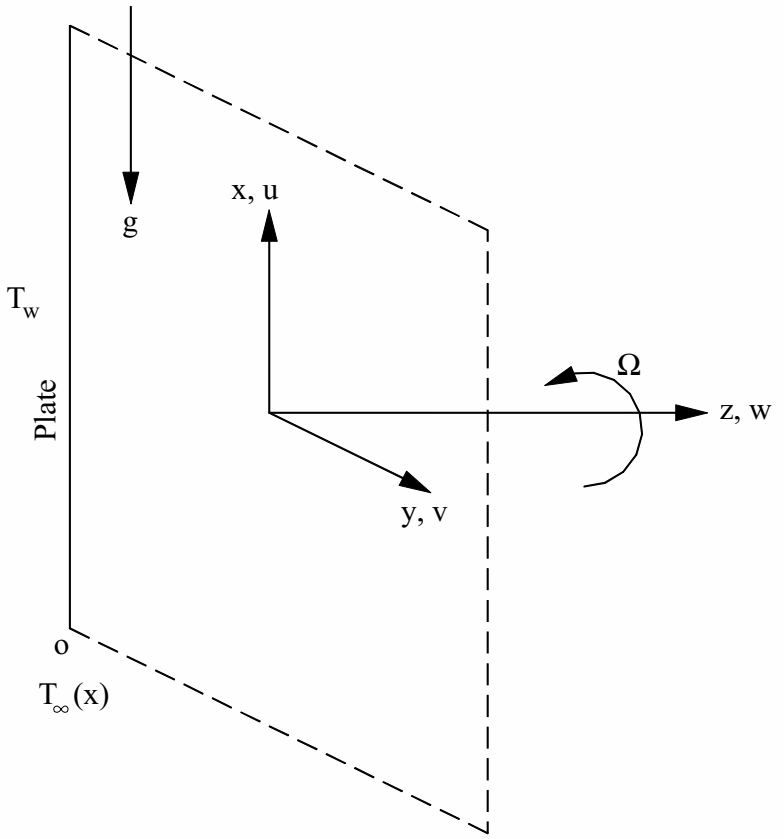

Fig. 1. Physical model and coordiante system.

z-axis which is horizontal (see Fig. 1). The gravity g acts downward in the negative x direction. The fluid properties are assumed to be constant except for the density variation, which gives rise to buoyancy forces. The field rotation gives rise to a secondary flow that makes the flow field three-dimensional, having velocity components u, v, and w along x, y, and z directions, respectively. Since the plate is along the x-axis, the flow and temperature fields are independent of y and only depend on x and z. We have considered the non-Darcy effects, which include inertia, boundary, and convective effects, using volume-averaged principles and empirical results [9]. The porous medium is assumed to be isotropic and homogeneous. Under the above assumptions along with the Boussinesq approximation, the boundary layer equations based on the conservation of mass, momentum, and energy, including the non-Darcy effects governing the natural convection flow of a rotating fluid over a vertical plate in a rotating coordinate system, can be expressed as [12, 19]

$$\frac{\partial u}{\partial x} + \frac{\partial w}{\partial z} = 0, \tag{1}$$

$$\epsilon^{-2}\left(u\frac{\partial u}{\partial x} + w\frac{\partial u}{\partial z} - 2\Omega v\right) = \epsilon^{-1}\nu\frac{\partial^2 u}{\partial z^2} - \frac{\nu}{K^*}u - C^* u^2 + g\beta(T - T_\infty), \tag{2}$$

$$\epsilon^{-2}\left(u\frac{\partial v}{\partial x} + w\frac{\partial v}{\partial z} + 2\Omega u\right) = \epsilon^{-1}\nu\frac{\partial^2 v}{\partial z^2} - \frac{\nu}{K^*}v - C^* v^2, \tag{3}$$

$$u\frac{\partial T}{\partial x} + w\frac{\partial T}{\partial z} = \alpha_e\frac{\partial^2 T}{\partial z^2}\,, \tag{4}$$

with the boundary conditions given by

$$\begin{aligned} u(x,0) = v(x,0) = w(x,\infty) = 0, \qquad & T(x,0) = T_w, \\ u(x,\infty) = w(x,\infty) = 0, \qquad & T(x,\infty) = T_\infty(x), \\ u(0,z), v(0,z) = 0, \qquad & T(0,z) = T_0. \end{aligned} \tag{5}$$

It is more convenient to deal with dimensionless equations. Hence, we apply the following transformations:

$$\begin{aligned} X = \frac{x}{L}\,, \qquad Z = \frac{z}{L\mathrm{Gr}_L^{-1/4}}\,, \\ U = \frac{u}{\nu L^{-1}\mathrm{Gr}_L^{1/2}}\,, \qquad V = \frac{v}{\nu L^{-1}\mathrm{Gr}_L^{1/2}}\,, \qquad W = \frac{w}{\nu L^{-1}\mathrm{Gr}_L^{1/4}}\,, \\ \theta = \frac{T - T_\infty}{T_w - T_0}\,, \qquad T_\infty = T_0 + ax, \qquad a = \frac{dT_\infty}{dx} > 0, \\ K = \frac{K^*}{L^2}\mathrm{Gr}_L^{1/2}, \qquad C = C^* L, \qquad S = \frac{aL}{T_w - T_0}\,, \\ \mathrm{Gr}_L = g\beta(T_w - T_0)\frac{L^3}{\nu^2}\,, \qquad \mathrm{Ro} = \frac{\Omega L^2}{\nu}\mathrm{Gr}_L^{1/2}, \qquad \mathrm{Pr} = \frac{\nu}{\alpha_e} \end{aligned} \tag{6}$$

to Eqs (1) – (4), and these reduce to

$$\frac{\partial U}{\partial X} + \frac{\partial W}{\partial Z} = 0, \tag{7}$$

$$\epsilon^{-2}\left(U\frac{\partial U}{\partial X}+W\frac{\partial U}{\partial Z}-2\mathrm{Ro}V\right)=\epsilon^{-1}\frac{\partial^2 U}{\partial Z^2}-K^{-1}U-CU^2+\theta, \tag{8}$$

$$\epsilon^{-2}\left(U\frac{\partial V}{\partial X}+W\frac{\partial V}{\partial Z}+2\mathrm{Ro}U\right)=\epsilon^{-1}\frac{\partial^2 V}{\partial Z^2}-K^{-1}V-CV^2, \tag{9}$$

$$U\frac{\partial\theta}{\partial X}+W\frac{\partial\theta}{\partial Z}+SU=\mathrm{Pr}^{-1}\frac{\partial^2\theta}{\partial Z^2}\,, \tag{10}$$

with boundary conditions

$$\begin{gathered}U(X,0)=V(X,0)=W(X,0)=0,\qquad \theta(X,0)=1-SX,\\ U(X,\infty)=V(X,\infty)=\theta(X,\infty)=0,\\ U(0,Z)=V(0,Z)=\theta(0,Z)=0,\qquad Z>0.\end{gathered} \tag{11}$$

In the absence of the rotation of the fluid ($\mathrm{Ro}=0$), Eqs (7), (8), and (10) under conditions (11) reduce to those of Chen and Lin [12]. For $\mathrm{Ro}=0$ the Eq. (9) is not required, because $V(X,Z)=0$.

The quantities of physical interest are the skin-friction coefficients and the Nusselt number (heat transfer coefficient)

$$\begin{aligned}C_{fx}&=\frac{\mu L^2}{\rho\nu^2\mathrm{Gr}_L}\left(\frac{\partial u}{\partial z}\right)_{z=0}=\mathrm{Gr}_L^{-1/4}\frac{\partial U(x,0)}{\partial Z}\,,\\ C_{fy}&=\frac{\mu L^2}{\rho\nu^2\mathrm{Gr}_L}\left(\frac{\partial v}{\partial z}\right)_{z=0}=\mathrm{Gr}_L^{-1/4}\frac{\partial V(x,0)}{\partial Z}\,,\\ \mathrm{Nu}&=-\frac{x}{T_w-T_\infty}\left(\frac{\partial T}{\partial z}\right)_{z=0}=-\mathrm{Gr}_L^{1/4}\frac{X}{1-SX}\,\frac{\partial\theta(X,0)}{\partial Z}\,,\\ \mathrm{Gr}_L^{-1/4}\overline{\mathrm{Nu}}&=-\int_0^1\frac{X}{1-SX}\,\frac{\partial\theta(X,0)}{\partial X}\,dX.\end{aligned} \tag{12}$$

2. Numerical Method

The nonlinear coupled parabolic partial differential equations (7) and (10) under conditions (11) have been solved numerically using an implicit, iterative, tri-diagonal finite-difference scheme similar to that discussed by Blottner [18]. The first-order derivatives with respect to X are replaced by two-point backward difference formulae of the form

$$\frac{\partial R}{\partial X}=\frac{1}{\Delta X}(R_{m,n}-R_{m-1,n}), \tag{13}$$

where R is the dependent variable for U or V or θ and m and n are the node locations along X and Z directions, respectively. The second-order partial differential equations for U, V, and θ are discretized by employing the three-point central-difference formulae, and the first-order equations

are discretized by using the trapezoidal rule. At each line of constant X, we get a system of algebraic equations. We evaluate the nonlinear terms in the equations at the previous iteration and solve the system of algebraic equations iteratively by using the Thomas algorithm [18]. The same procedure is followed for the next X value, and the equations are solved line by line until the desired X value is reached. The convergence criterion based on the relative difference between the current and the previous iterations has been used. When this difference reaches 10^{-5}, the solution is assumed to have converged and the iterative process is terminated.

The grid size ΔX and ΔZ is varied. For grid size less then 60×100, the numerical values differ only in the fourth decimal place. This corresponds to an error of $< 0.5\ \%$. We have taken the grid size 120×200 for the results presented.

3. Results and Dscussion

Eqs (7) – (10) under conditions (11) have been solved numerically using the method described earlier. In order to assess the accuracy of our method, we have compared the average Nusselt number ($\mathrm{Gr}_L^{-1/4}\overline{\mathrm{Nu}}$) values for $\mathrm{Ro} = 0$ to those of Chen and Lin [12] and found them in very good agreement. The comparison is shown in Fig. 2.

The effects of the thermal stratification parameter S on the velocity and temperature profiles (U, V, W, θ) for $\mathrm{Ro} = 0.5$, $K = X = 1$, $C = 0$, $\mathrm{Pr} = 5.4$, and $\epsilon = 0.9$ are shown in Figs 3 – 6. In general, an increase in the thermal stratification S reduces the momentum and thermal boundary layers. Consequently, the velocities in the X and Y directions (U, V) decrease with increasing S. The velocity component in the Z direction W is < 0 for $S < 0.2$ and $W > 0$ for $S > 0.2$. This implies that the axial velocity W is directed toward the plate for $S < 0.2$ (inflow) and away from it

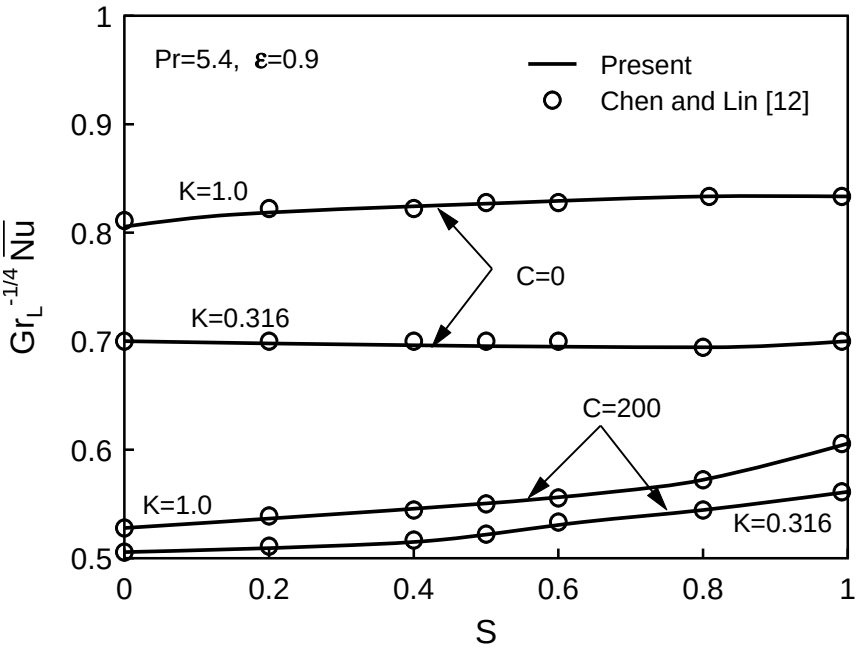

Fig. 2. Comparison of the average Nusselt number $\mathrm{Gr}_L^{-1/4}\overline{\mathrm{Nu}}$.

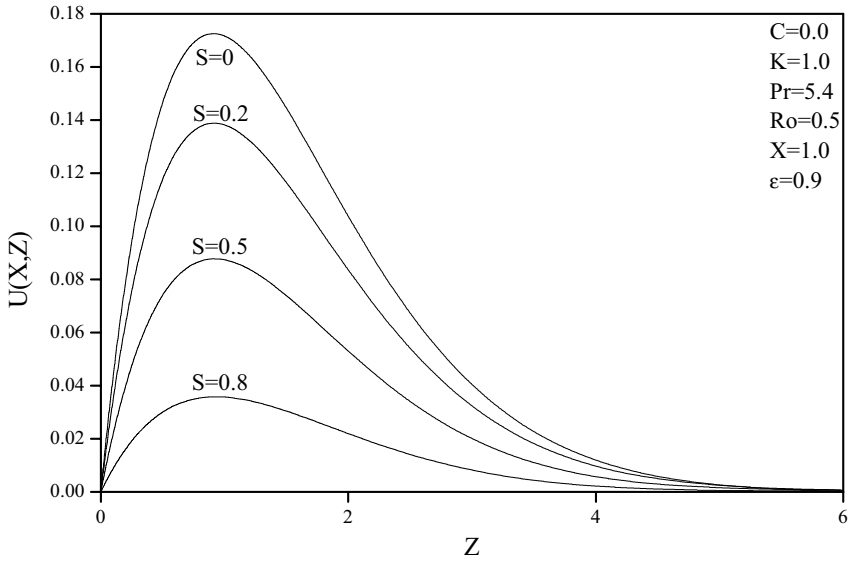

Fig. 3. Effects of S on $U(X, Z)$.

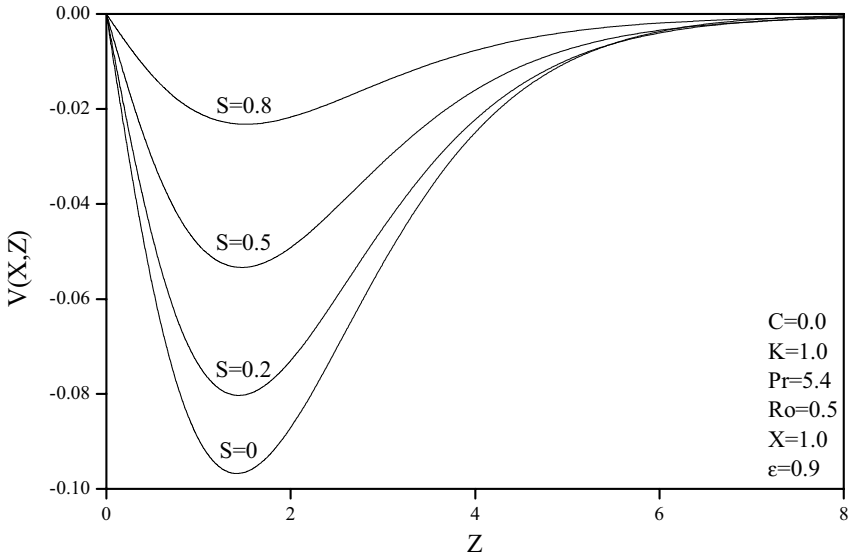

Fig. 4. Effects of S on $V(X, Z)$.

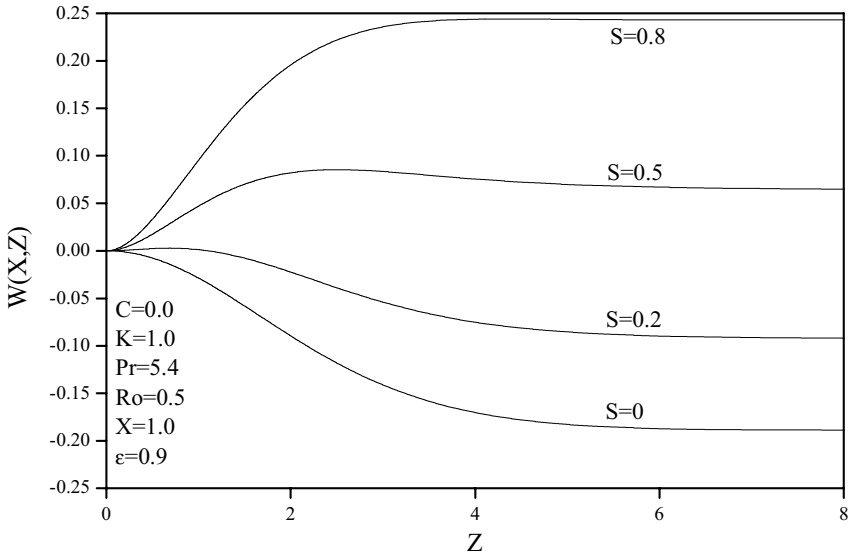

Fig. 5. Effects of S on $W(X, Z)$.

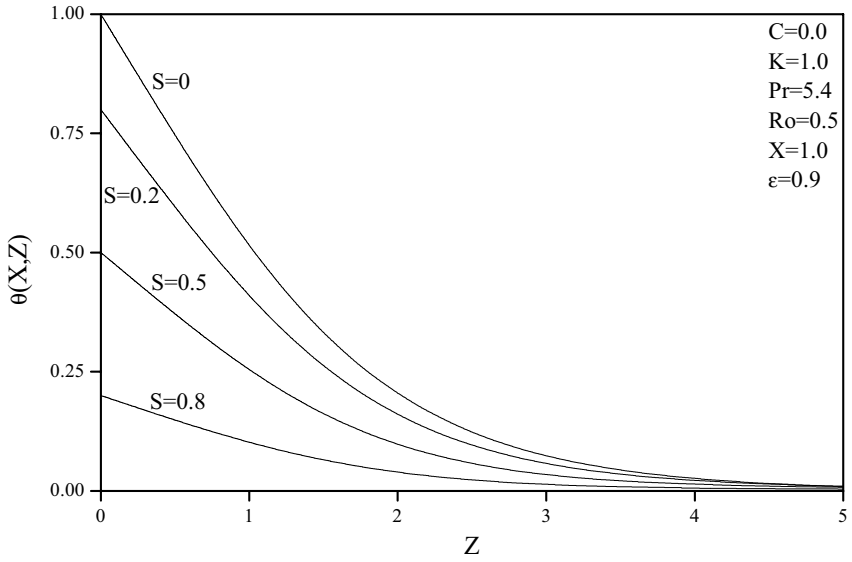

Fig. 6. Effects of S on $\theta(X, Z)$.

for $S > 0.2$ (outflow). The velocity components U and V tend to zero exponentially at the edge of the boundary layer ($Z \to \infty$) for all S. In addition, the temperature θ in the presence ($S \neq 0$) or absence ($S = 0$) of thermal stratification also decays to zero as $Z \to \infty$ in an exponential manner. The temperature θ decreases everywhere (except at $X = 0$) as S increases because an increase in S also implies a reduction in the wall temperature. Thus, the thermal stratification exerts a strong influence on the velocity and temperature profiles.

The effects of the thermal stratification parameter S on the skin-friction and heat transfer coefficient ($\mathrm{Gr}_L^{1/4} C_{fx}$, $\mathrm{Gr}_L^{1/4} C_{fy}$, $\mathrm{Gr}_L^{-1/4}\mathrm{Nu}$) for $\mathrm{Pr} = 5.4$, $\epsilon = 0.9$, $\mathrm{Ro} = 0.5$, $K = 1$, $C = 0$ are presented in Figs 7 – 9. The effects of S become more pronounced as X increases because S is multiplied by X in the boundary conditions (see Eq. (11)) and by U in Eq. (10), i. e., $U = 0$ at $X = 0$ and 1). As mentioned earlier, the momentum and thermal boundary layers reduce with increasing S, the skin-friction coefficient in the X direction ($\mathrm{Gr}_L^{1/4} C_{fx}$) and heat transfer coefficient $\mathrm{Gr}_L^{-1/4}\mathrm{Nu}$) increase with S, whereas the skin-friction coefficient in the Y direction ($\mathrm{Gr}_L^{1/4} C_{fy}$) decreases. For $S < 0.2$, the skin-friction coefficient in the X direction increases with X, but for $S \geq 0.2$, it first increases and then decreases. This trend is attributed to the competition between various parameters.

Figs 10 – 13 display the effects of the Rossby number Ro on the velocity and temperature profiles (U, V, W, θ) for $\mathrm{Pr} = 5.4$, $S = 0.5$, $\epsilon = 0.9$, $K = X = 1$, $C = 0$. Since the Rossby number Ro gives rise to secondary flow ($V = 0$ for $\mathrm{Ro} = 0$), the secondary flow velocity V increases with Ro, but, in general, the primary flow velocities (U, W) decrease. As Ro increases from zero up to $\mathrm{Ro} = 0.5$, the momentum boundary layer decreases. However, for $\mathrm{Ro} > 0.5$, it increases. On the other hand, the thermal boundary layer grows with increasing values of Ro. Hence, temperature θ increases with Ro. The temperature profiles show exponential decay to the free-stream conditions as mentioned earlier.

Figs 14 – 16 present the effects of the Rossby number Ro on the skin-friction coefficients and Nusselt number ($Gr_x^{1/4} C_{fx}$, $\mathrm{Gr}_L^{1/4} C_{fy}$, $\mathrm{Gr}_L^{-1/4}\mathrm{Nu}$) for $\mathrm{Pr} = 5.4$, $S = 0.5$, $\epsilon = 0.9$, $K = 1$, $C = 0$. The effect of Ro on the skin friction and Nusselt number is more pronounced away from the leading edge of the plate. Both the skin-friction coefficient in the X direction and the Nusselt number decrease with increasing values of Ro, but the skin-friction coefficient in the y direction increases. This is due to the growth of the secondary flow with increasing Ro. Since Ro opposes the motion in the x direction (see Eq. (8)), the skin-friction coefficient in the x direction as well as the Nusselt number decrease with increase Ro, but the skin-friction coefficient in the y direction increases, because Ro supports the motion in that direction (see Eq. (9)). For a fixed Ro, $Gr_x^{1/4} C_{fx}$, and $\mathrm{Gr}_L^{1/4} C_{fy}$ first increase with X, then decrease, whereas $\mathrm{Gr}_L^{-1/4}\mathrm{Nu}$, continuously increases with X.

The effects of the porosity ϵ on the Nusselt number ($\mathrm{Gr}_L^{-1/4}\mathrm{Nu}$) for $\mathrm{Pr} = 5.4$, $\mathrm{Ro} = S = 0.5$, $K = 1$, and $C = 0$ are shown in Fig. 17, and they increase with X. The Nusselt number increases with porosity ϵ, because an increase in ϵ implies less resistance to the fluid motion ($\epsilon = 1$ for uniform medium). Hence, fluid accelerates with increasing ϵ, which takes away more heat from the surface. Consequently, the thermal boundary layer decreases. This enhances the Nusselt number as ϵ increases. The porosity ϵ has a strong influence on the Nusselt number, which increases by ~ 95 % as ϵ increases from 0.5 to 0.9.

The effects of the permeability parameter K on $\mathrm{Gr}_L^{-1/4}\mathrm{Nu}$ for $\mathrm{Pr} = 5.4$, $S = 0.5$, $\epsilon = 0.9$, $C = 0$, $\mathrm{Ro} = 0.5$, and 1.25 are displayed in Fig. 18. The increase in K implies less resistance to the fluid motion by the porous medium, which results in a thinner thermal boundary layer. Hence, the Nusselt number increases when $\mathrm{Ro} = 0.5$. When $\mathrm{Ro} = 1.25$, this trend is reversed because the

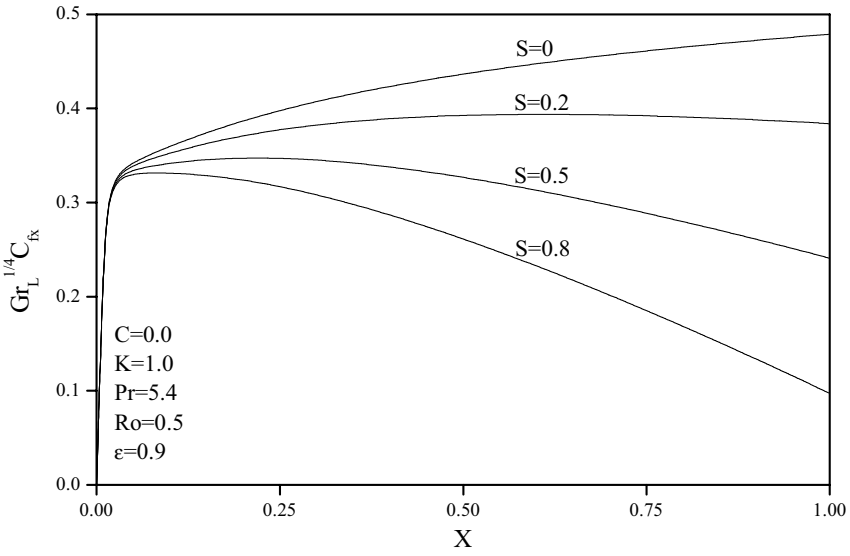

Fig. 7. Effects of S on $\mathrm{Gr}_L^{1/4} C_{fx}$.

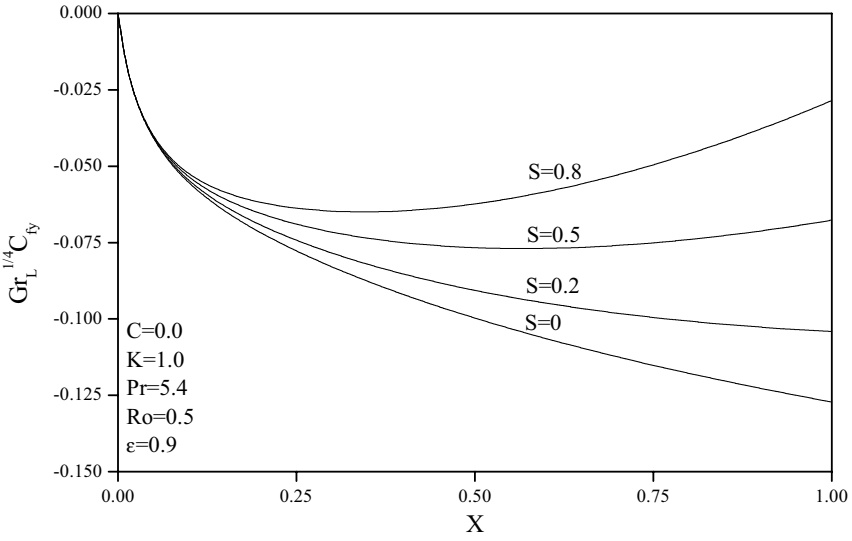

Fig. 8. Effects of S on $\mathrm{Gr}_L^{1/4} C_{fy}$.

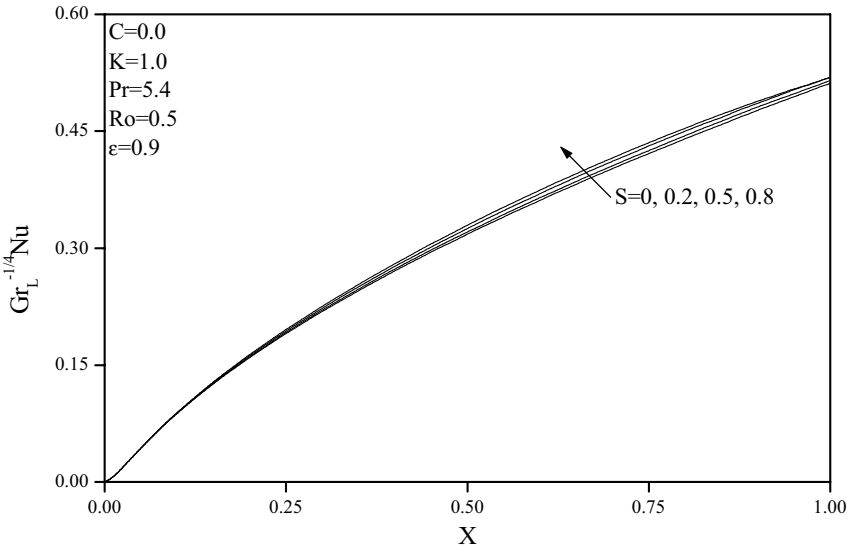

Fig. 9. Effects of S on $\mathrm{Gr}_L^{1/4}\mathrm{Nu}$.

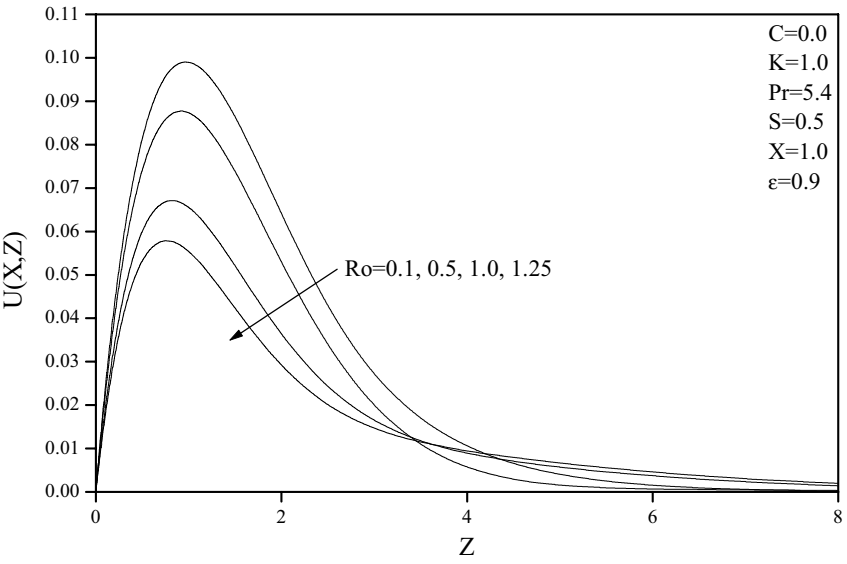

Fig. 10. Effects of Ro on $U(X, Z)$.

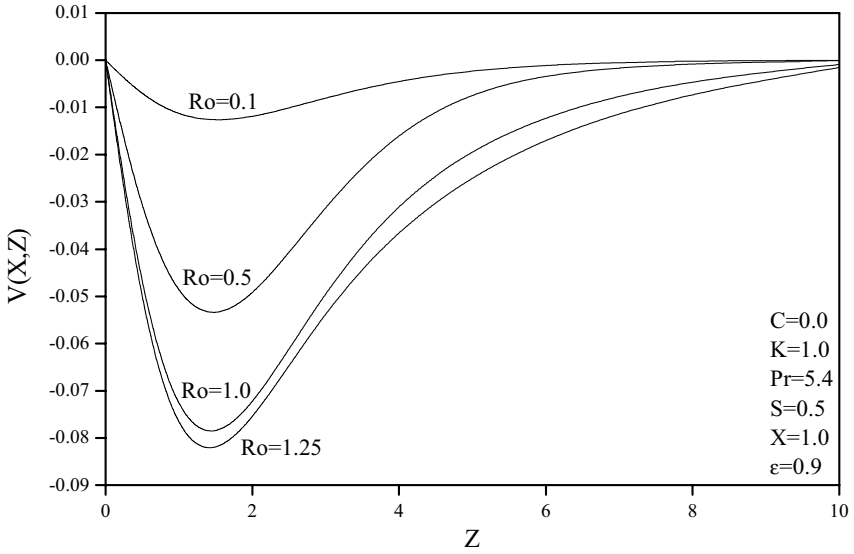

Fig. 11. Effects of Ro on $V(X, Z)$.

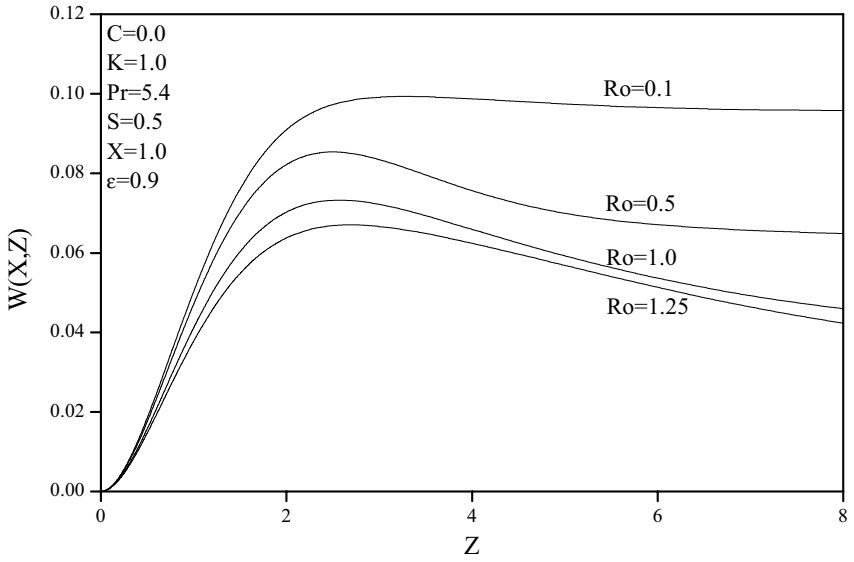

Fig. 12. Effects of Ro on $W(X, Z)$.

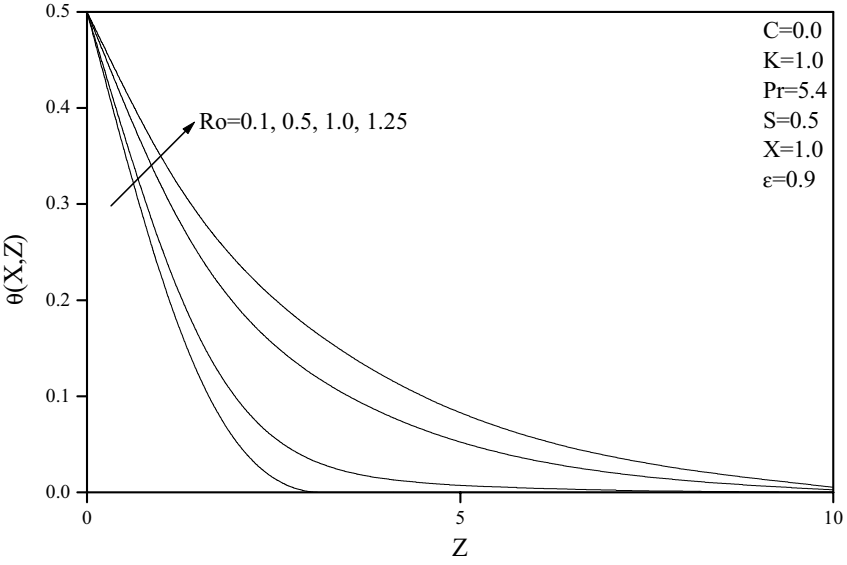

Fig. 13. Effects of Ro on $\theta(X, Z)$.

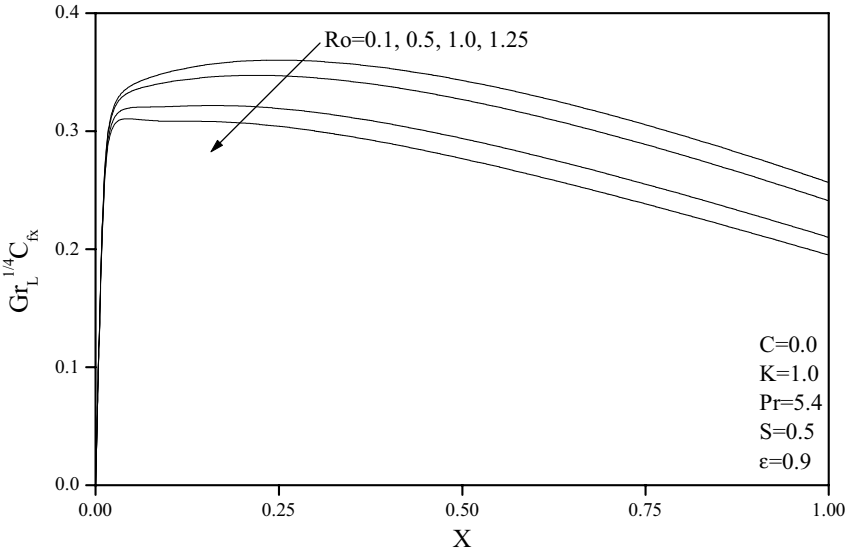

Fig. 14. Effects of Ro on $\mathrm{Gr}_L^{1/4} C_{fx}$.

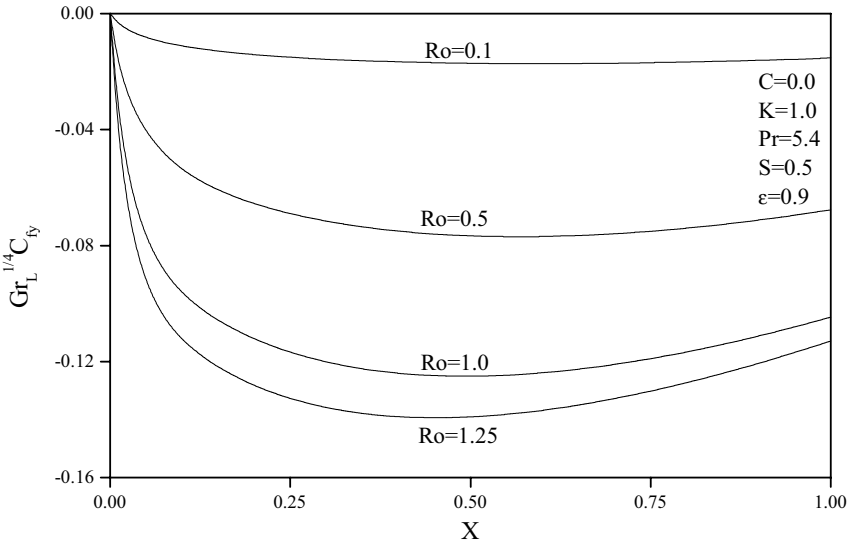

Fig. 15. Effects of Ro on $\mathrm{Gr}_L^{1/4}C_{fy}$.

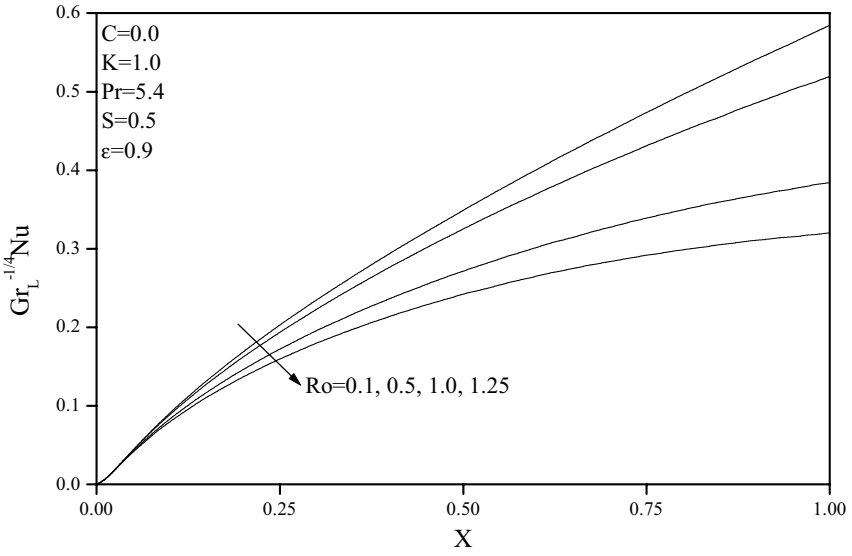

Fig. 16. Effects of Ro on $\mathrm{Gr}_L^{-1/4}\mathrm{Nu}$.

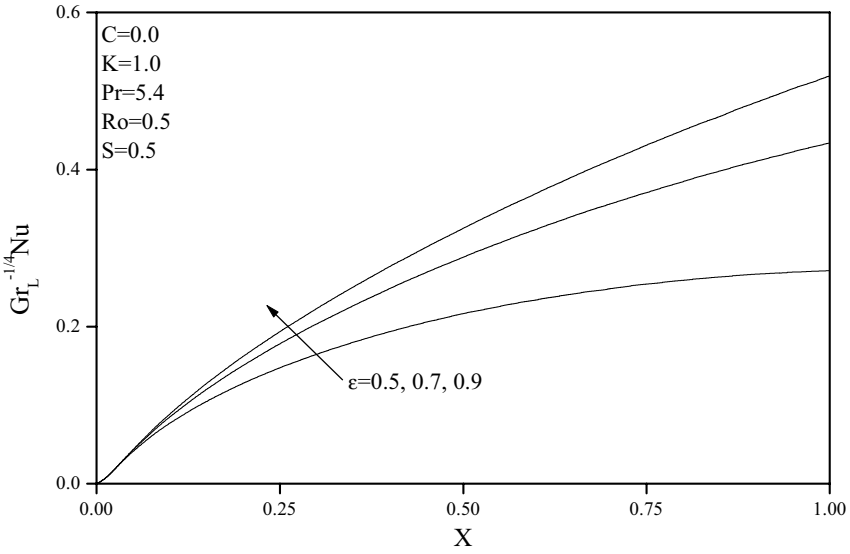

Fig. 17. Effects of ϵ on $\mathrm{Gr}_L^{-1/4}\mathrm{Nu}$.

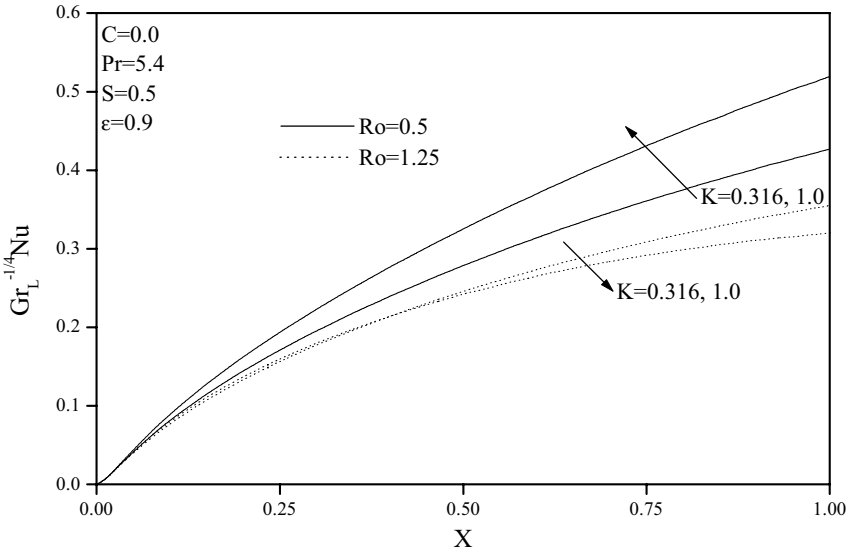

Fig. 18. Effects of K on $\mathrm{Gr}_L^{-1/4}\mathrm{Nu}$.

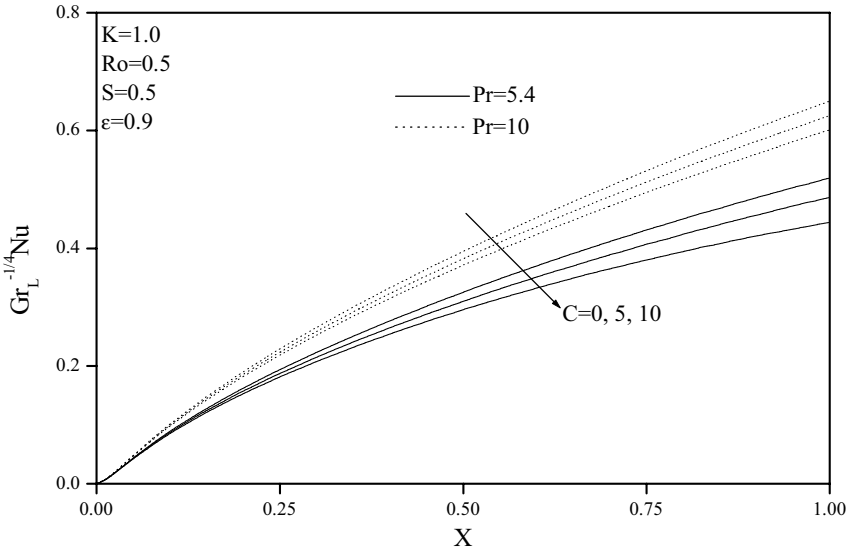

Fig. 19. Effects of Pr and C on $\mathrm{Gr}_L^{-1/4}\mathrm{Nu}$.

thermal boundary grows more rapidly with Ro than its reduction caused by an increase in K. The Nusselt number depends weakly on K. It increases by $\sim 4\,\%$ as K increases from 0.316 to 1, when $\mathrm{Ro} = 0.5$.

Finally, Fig. 19 illustrates the influence of the inertia parameter C for two values of the Prandtl number Pr ($\mathrm{Pr} = 5.4$ and 10) and $S = 0.5$, $\epsilon = 0.9$, $K = 1$, and $\mathrm{Ro} = 0.5$. The Nusselt number $\mathrm{Gr}_L^{-1/4}\mathrm{Nu}$ decreases with increasing inertia parameter C because the momentum and thermal boundary layers become thick due to the increase in the resistance to the motion. In addition, increasing Pr has the tendency to decrease the thermal boundary layer, resulting in increases in the local Nusselt number $\mathrm{Gr}_L^{-1/4}\mathrm{Nu}$. These behaviors are clearly shown in Fig. 19.

Conclusions

The thermal stratification of the fluid, Rossby number, and the porosity of the medium have strong influence on the flow and temperature fields. The skin friction in the x direction and the Nusselt number increase with the thermal stratification, but the skin friction in the y direction decreases. The effects of the Rossby number are also opposite those of the thermal stratification in which the Nusselt number decreases with increases in the Rossby number. In the presence of thermal stratification, the temperature profiles as well as the velocity profiles decay to zero, exponentially, at the edge of the boundary layer. Beyond a certain value of Rossby number ($\mathrm{Ro} > 0.5$), the momentum boundary layer increases as the Rossby number increases, whereas it decreases as Ro is increased from zero to 0.5.

REFERENCES

1. Cheng, P., Heat Transfer in Geothermal Systems, *Adv. Heat Transfer*, 1978, **14**, pp. 1–105.
2. Cheng, P., Natural Convection in a Porous Medium: External Flows, In: *NATO ASI Natural Convection*, Izmir, Turkey, July 16–27, 1984.
3. Catton, I., Natural Convection Heat Transfer in Porous Media, In: *Natural Convection: Fundamentals and Applications*, W. Aung, S. Kakac, and S. Viskanta, Eds, Hemisphere, New York, 1985.
4. Pop, I., Ingham, D. B., and Merkin, J. H., Unsteady Free and Mixed Convection in External Flows, *Adv. Fluid Mech., Transient Convection Heat Transfer in External Flow*, 1998, **19**, pp. 83–114.
5. Nield, D. A. and Bejan, A., *Convection in Porous Media*, Springer, New York, 1999.
6. Vafai, K., Ed., *Handbook of Porous Media*, Marcel Dekker, New York, 2000.
7. Pop, I., and Ingham, D. B., *Convective Heat Transfer; Mathematical and Computational Modelling of Viscous Fluids and Porous Media*, Pergamon Press, Oxford, 2001.
8. Ingham, D. B., and Pop, I., Eds, *Transport Phenomena in Porous Media*, Pergamon Press, Oxford, 2002.
9. Tien, C. L. and Vafai, K., Convective and Radiative Heat Transfer in Porous Media, *Adv. Appl. Mech.*, 1989, **27**, pp. 225–281.
10. Chen, C. K., Hung, C. I., and Horng, H. C., Transient Natural Convection on a Vertical Flat Plate Embedded in a High Porosity Medium, *ASME J. Energy Resch Technol.*, 1987, **109**, pp. 112–118.
11. Singh, P. and Tiwari, K., Non-Darcy Free Convection from Vertical Surfaces in Thermally Stratified Porous Media, *Int. J. Engng Sci.*, 1993, **31**, pp. 1233–1242.
12. Chen, C. K. and Lin, C. R., Natural Convection from an Isothermal Vertical Surface Embedded in a Thermally-Stratified High-Porosity Medium, *Int. J. Engng Sci.*, 1995, **33**, pp. 131–138.
13. Chamkha, A. J., Hydromagnetic Natural Convection from an Isothermal Inclined Surface Adjacent to a Thermally Stratified Porous Medium, *Int. J. Engng Sci.*, 1997, **35**, pp. 975–996.
14. Minto, B. J., Ingham, D. B., and Pop, I., Free Convection Driven by an Exothermic Reaction on a Vertical Surface Embedded in Porous Media, *Int. J. Heat Mass Transfer*, 1998, **41**, pp. 11–24.
15. Jung, C. J., Chen, C. H., and Chen, C. B., Non-Darcy Free Convection Along a Non-Isothermal Vertical Surface in a Thermally Stratified Porous Medium, *Int. J. Engng Sci.*, 1999, **37**, pp. 477–496.
16. Rees, D. A. S. and Pop, I., Vertical Free Convection in a Porous Medium with Variable Permeability Effect, *Int. J. Engng Sci.*, 2000, **38**, pp. 2565–2592.
17. Takhar, H. S., Chamkha, A. J., and Nath, G., Natural Convection on a Vertical Cylinder Embedded in a Thermally Stratified High-Porosity Medium, *Int. J. Therm. Sci.*, 2002, **41**, pp. 83–93.
18. Blottner, F. G., Finite-Difference Methods of Solution of Boundary Layer Equations, *AIAA J.*, 1970, **8**, pp. 193–205.
19. Vadasz, P., *Flow in Rotating Porous Media*, Computational Mechanics Publ., Southamption, UK, 1997, pp. 161–213.

□◆◆◆□